Astron. Astrophys. 330, 351–358 (1998)

ASTRONOMY
AND
ASTROPHYSICS

Non-thermal hydrogen line emission caused by an oblique incident proton beam through charge exchange

X. Zhao[1], **C. Fang**[1,2], **and J.-C. Hénoux**[2]

[1] Department of Astronomy, Nanjing University, Nanjing, P.R. China
[2] Observatoire de Paris, DASOP, CNRS-URA 2080, Meudon, France

Received 4 August 1997 / Accepted 18 September 1997

Abstract. In this paper, formulae are given for computing the non-thermal emission of superthermal hydrogen atoms generated through charge exchange by the bombardment of the solar atmosphere by an oblique incident proton beam with a given pitch angle. Specifically, we discuss the non-thermal emission of hydrogen in Lyα , Lyβ, and Hα lines and find that the profiles of these lines are quite different from the ones caused by bombardment by a proton beam moving vertically. The intensity and the asymmetry of the non-thermal emission profiles strongly depend on the beam pitch angle α and on the angle θ between the direction of magnetic field and the line of sight. By computing the thermal emission under the semi-empirical flare atmospheric models F1, F2, and the quiet-Sun atmospheric model C, we compare the relative importance of thermal and non-thermal emission. For the Hα line, the non-thermal emission, with the proton flux used, is too small to be detectable; for the Lyα line, the contribution of non-thermal emission to the line wings is smaller than the one of a vertical beam; while for the Lyβ line, line wing enhancement and broadening are significant. Thus, Lyβ line is a good diagnostic tool for non-thermal proton beam bombardment.

Key words: line: profiles – atomic processes – Sun: flares

1. Introduction

The study of the energy transport mechanisms is of major interest in the understanding of solar flares since it provides information on the amount and nature of the energy released in flares. In the 1940's, Giovanelli & Ellison (cf. Brown et al. 1990) firstly suggested that energetic particles might play an important role in this process. Hard X-ray emission due to electron Bremsstrahlung is present in most flares. Neupert (1968) pointed out that, for most flares, the soft X-ray emission measure is roughly proportional to the time integrated hard X-ray intensity. This finding leads to the thick-target model (Brown 1971, Syrovatskii & Shmeleva 1971). The ratio between the rate of energy loss in Coulomb collision and in Bremsstrahlung emission being close to 10^5, energetic electrons emitting hard X-ray deposit in the solar atmosphere an energy orders of magnitude higher than the one they radiate in X-rays. Inversion of the hard X-ray spectrum, assuming that the hard X-ray emitting electrons collide with the cold solar chromosphere, provides the electron spectrum. Consequently as pointed out in Emslie et al. (1996) (see also Canfield et al. 1986), over the last decades, several models of the interaction of high energy electrons with the solar atmosphere have been published that provide estimations of various observable signatures. For suitably impulsive hard X-ray events, energetic electrons appear to be responsible for atmospheric heating.

Beams of high energy electrons cannot explain the atmospheric heating in all observed flares. Following Dennis (1988) three categories of flares can be distinguished, one typically impulsive with hard X-ray spikes on times scales of seconds, where a good correlation is found between hard and soft X-ray emissions, and two others with a more gradual variation of hard X-ray emission. In flares with rather gradual hard X-ray emission or without hard X-ray emission at all, soft X-ray emission can be present either long time after the hard X-ray emission or before this emission. For these flares another source of energy deposit than energetic electrons is required (Feldman et al. 1982, Dennis et al. 1993, Dennis & Zarro 1993, Zarro et al. 1995, Doschek et al. 1996). Heating by a DC-electric field has been suggested by Zarro et al. (1995) to explain a strong stationary component of soft X-ray Ca XIX emission present at the start of impulsive hard X-ray emission. Proton beams must be also considered as a potential source of heating in solar flares.

Two facts are supporting the proton beam hypothesis. First, for a given particle velocity, protons have higher individual energies than light electrons, and can therefore carry the same power for a lower particle flux than electrons, so the proton beam model is electrodynamically less demanding. Secondly, γ-ray observations suggest that the proton energy spectrum below 10 MeV may be considerably steeper than previously thought. Bessel function spectra used usually to describe the energetic proton

Send offprint requests to: J.-C. Hénoux

spectrum do not provide a satisfactory explanation of observed γ ray lines fluences. Share & Murphy (1995) have shown that the ratio of the 1.63 Mev ^{20}Ne line to the 6.13 MeV ^{16}O line fluence increases as the proton accelerated spectrum becomes softer. They suggested that the observed high Ne/O line ratio may be due not to enhanced Ne abundance but rather to the low energy production threshold of the 1.63 Mev ^{20}Ne line compared to the 6.13 MeV ^{16}O line. Ramaty et al. (1995) found that in order to avoid values of the Ne/O abundance ratio greater than twice the coronal value 0.15 in the γ ray line production region, the accelerated proton energy spectrum should be as steep as an unbroken power law. In such case the energy contained in ions above 1 MeV would range from about 10^{30} to 10^{32} ergs and would then be comparable to or even exceed the energy contained in the energetic electrons producing hard X-ray. Since γ-ray line observations suggest that 1 MeV protons may play a dominant role in the energetic of solar flares, all methods to detect low energy protons must be revisited.

Several diagnostic methods for low energy protons (E $\leq$ 1 Mev) have been developed. Apart from building very large future γ-ray detectors for protons with an energy around and below 1 Mev, three diagnostic methods could be used:

- The first diagnostic is based on the property of proton beams, contrary to electrons, of keeping their anisotropic velocity angular distribution when bombarding the solar chromosphere. Consequently they can, by collisional excitation, generate polarized line emission and such polarization has been observed in events with long duration gradual soft X-ray emission (Hénoux et al. 1990, Vogt & Hénoux 1996).

- The Hα line profile can also be used as diagnostic for low energy protons. Contrary to electrons that deposit their energy down to the low chromosphere and lead to enhanced line wing emission (Fang, Hénoux and Gan 1993), protons deposit their energy in the highest chromospheric layers in collisional excitation and ionization of neutral hydrogen. This enhances Hα line center emission and eliminates the line central reversal (Hénoux, Fang and Gan 1993). However, a very high pressure in the corona can produce the same effect, which makes this diagnostic method ambiguous.

- A third possible diagnostic for low energy protons, that is developed in this paper, is based on proton-hydrogen charge exchange. Orral & Zirker (1976) pointed out that, by proton-hydrogen charge exchange, proton beam bombardment could produce Doppler shifted emissions of the recombined protons and hence enhancements of the line wings of chromospheric lines. They suggested that consequently the Lyα line could be used as a diagnostic of proton bombardment. Canfield & Chang (1985, thereafter referred to as CC) investigated the ionization effect caused by a proton beam and computed the enhancement of Hα and Lyα lines produced by a vertical proton beam. They concluded that the non-thermal emission of the Hα line is less than the background and not detectable, while the intensity of the Lyα red wing is an order of magnitude higher than the background. Using more recent atomic data and refined atmospheric models, Fang et al. (1995), thereafter referred to as FFH, computed the non-thermal emission of hydrogen in Hα, Lyα and Lyβ lines for the case of vertical bombardment. They confirmed that the Hα non-thermal emission is too small to be detectable, but the Lyα and Lyβ lines could be used to diagnose the proton beam bombardment. However, as their results showed, this kind of enhancement will be more obvious at the beginning of the flare, decreasing with the increase of the column mass that accompanies the chromospheric evaporation produced by the proton bombardment.

In this paper, the non-thermal emission of the super-thermal hydrogen atoms produced by charge exchange between energetic protons and neutral hydrogen atoms, when an oblique incident proton beam is bombarding the chromosphere, is computed for different semi-empirical flare models and for the quiet-Sun model. In Sect. 2, we introduce the theoretical formulas. Sect. 3 gives the result of our analysis, followed by a conclusion given in Sect. 4.

2. Theoretical formulas

In order to solve this problem quantitatively, the following simplifications have been made: first we represent the proton energy distribution spectrum before its penetration in the solar chromosphere as a time independent power law; secondly, the photons emitted by the superthermal hydrogen atoms formed in the charge exchange process are supposed to escape from the solar atmosphere without being absorbed. This hypothesis is valid for photons outside a narrow wavelength band centered on the unshifted line center with a half-width of about 2 Å.

2.1. Calculation of superthermal hydrogen number density

When an incident proton beam precipitates on a neutral hydrogen target in solar atmosphere, a proton H_b^+ in the beam may capture an electron from a target hydrogen atom. This proton becomes a superthermal hydrogen atom $H_{j,b}$ excited to level j. The charge exchange process can be written as:

$$H_b^+ + H \leftrightarrow H_{j,b} + H^+. \tag{1}$$

To compute the non-thermal line emission intensity produced in charge exchange, the number density of the superthermal hydrogen atoms at different energy levels is needed. According to FFH, the populations of the various j levels of the superthermal hydrogen atoms are given by the statistical equilibrium equations

$$D_j n_j = C_{pj} n_p + \sum_{i<j} C_{ij} n_i + \sum_{k>j} C_{kj} n_k \tag{2}$$

for all j, where D_j is the destruction rate per atom in level j, C_{pj} the charge exchange rate to level j, C_{ij} and C_{kj} are respectively the collisional excitation and deexcitation rates of fast hydrogen atoms, together with the conservation equation of superthermal particles given by

$$F(E,z) = \sum_j n_j v. \tag{3}$$

Here, F(E,z) is the flux of energetic hydrogen atoms, that can be taken equal to the proton flux in absence of the charge exchange, and v is the velocity of the energetic particles. Superthermal particles are decelerated by Coulomb collisions. We assume that at the accelerating site in the corona the energy distribution of the flux, F(E_0, z_0), of energetic particles with an energy E_0 is represented by a power law

$$F(E_0, z_0) \propto E_0^{-\delta}, \tag{4}$$

above an energy cut-off E_c. As given in CC and FFH, after crossing a column number density N, the energy distribution of the proton beam flux at a depth z is given by

$$F(E, z) = (\delta - 2)\mathscr{F}_1 E_c^{\delta-2} E(E^2 + E_N^2)^{-(\delta+1)/2}, \tag{5}$$

where E_N is the energy needed for a proton to cross a column density N and $\mathscr{F}_1$ is the energy flux above the low energy cutoff E_c. The minimum energy E_m of the proton energy distribution at a depth z is given by

$$E_m = \sqrt{(E_c^2 - E_N^2)} \text{ when } E_c \geq E_N \tag{6}$$

$$E_m = 0 \text{ when } E_c \leq E_N . \tag{7}$$

The computation of the above coefficients are the same as in FFH.

2.2. Proton propagation

Using the classical theory of scattering under the Coulomb potential of both charges and neutral particles, Emslie (1978) has derived formulae for the mean scattering of a beam of charged particles interacting with a cold hydrogen target. The formulae giving the variation of the mean velocity component v_x parallel to the axis that defines the Lagrangian column density N must be corrected for electrons and protons, in order to take into account the variation of v_x due to inelastic collisions. This leads

for electrons to:

$$\frac{dv_x}{dN} = \frac{-Kv_x}{2\mu E^2}\left[3x\Lambda + (1-x)(\Lambda' + 2\Lambda'')\right], \tag{8}$$

and for protons to:

$$\frac{dv_x}{dN} = \frac{-Kv_x}{2\mu E^2}\left[\left(\frac{m_p}{m_e}\right)(x\Lambda + (1-x)\Lambda') + \frac{1}{2}(1-x)(\Lambda'')\right], \tag{9}$$

where x is the hydrogen target ionization degree. Λ represents the effects of inelatic collisions on electrons and protons. Λ' and Λ'' represents respectively the effects of the inelastic and elastic collisions on neutral hydrogen atoms. $K = 2\pi e^4$ and $\mu = v_x/v$. The energy loss per element of column density dN is taken from Emslie:

$$\frac{dE}{dN} = \frac{-K}{\mu E}\left(\frac{m}{m_e}\right)\left[x\Lambda + (1-x)\Lambda'\right], \tag{10}$$

where m is the mass of the propagating particle, i.e. m_e or m_p. For protons, it can be seen from Eq. (9) that the contribution of scattering to the change of v_x is negligible since Λ' and Λ'' are of the same order of magnitude. Following Emslie, Eqs. (9) and (10) lead to:

$$\frac{dE}{dv_x} = \frac{2E}{v_x} \quad \text{or} \quad E = E_0(v_x/v_{x0})^2. \tag{11}$$

Since

$$\frac{v_x}{v_{x0}} = \frac{\mu}{\mu_0}\left(\frac{E}{E_0}\right)^{1/2} \quad \text{(Eq. (28) in Emslie 1978)}, \tag{12}$$

we obtain

$$\frac{\mu}{\mu_0} = 1, \tag{13}$$

that shows that protons are not deviated.

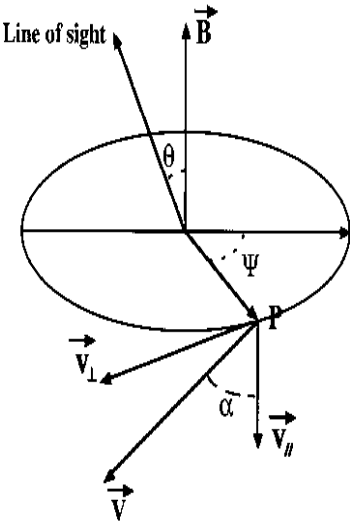

Fig. 1. Geometry of a proton beam moving with a pitch angle α along a vertical magnetic field at a location of heliocentric angle θ. The angle ψ defines the proton position around the magnetic field

2.3. Photon emission

We consider a proton beam propagating with a pitch angle α along an uniform and vertical magnetic field. The position of a proton on its trajectory is defined by its vertical column density and by the angle ψ that gives its location around the magnetic field. The geometry of the beam is represented in Fig. 1. The velocity along the line of sight is given by

$$v' = v\,(\cos\alpha\cos\theta - \sin\alpha\sin\theta\ \sin\psi)\,, \tag{14}$$

where θ, as usual, is the heliocentric angle. The resulting wavelength shift $\Delta\lambda$ is

$$\Delta\lambda = v'\frac{\lambda}{c} = \sqrt{\frac{2E}{m}}\frac{\lambda}{c}[\cos\alpha\cos\theta - \sin\alpha\sin\theta\sin\psi]. \tag{15}$$

In these equations, E is the particle energy and m the proton mass. The angle ψ is counted positively in the direction of rotation of the protons around a vertical axis; its origin is in the plane

defined by the local solar vertical and the line of sight. As shown by formulae 14 and 15, protons having positions symmetrical around the vertical plane perpendicular to the one containing the line of sight ($\psi = \pm\pi/2$) produce identical wavelength shifts. Therefore, in all what follows, ψ shall vary from $-\pi/2$ to $+\pi/2$.

The wavelength shift is usually positive. However, in configurations such that $\tan\alpha\tan\theta \geq 1$, it can be negative for $\psi_1 < \psi < \pi/2$, where $\psi_1 = \arcsin(1/\tan\alpha\tan\theta)$. Consequently, as detailed later, two cases must be considered, corresponding respectively to the rotation angle ψ being inside or outside the interval $\psi_1 \leftrightarrow \pi/2$.

The rotating superthermal atoms formed by charge exchange emit Doppler shifted photons when deexciting from the energy level j to the level i. Defining $n_j(E,z)dzdEd\psi/2\pi$ the phase-space number density of superthermal hydrogen atoms excited to the level j, in the distance range $z \leftrightarrow z+dz$, energy range $E \leftrightarrow E+dE$, and in the interval of rotation angle $\psi \leftrightarrow \psi + d\psi$, the contribution to the photon emission rate at a wavelength displacement $\Delta\lambda$ from line center of protons in these depth, energy and rotation angle ranges, is given by

$$d\Phi_{ji}(\Delta\lambda)\,d(\Delta\lambda) = n_j(E,z)\frac{A_{ji}}{4\pi}dE\,dz\frac{d\psi}{2\pi}, \tag{16}$$

where A_{ji} is the emissivity per steradian. Protons in the rotation angle range $\psi \leftrightarrow \psi + d\psi$ and in the energy band $E \leftrightarrow E + dE$, leads by the desexcitation of the hydrogen atoms formed after charge exchange to the emission of photons distributed over a spectral range $\Delta\lambda \leftrightarrow \Delta\lambda + d\Delta\lambda$. As derived from Eq. (15), $d\Delta\lambda = dE\Delta\lambda/(2E)$. Consequently

$$d\Phi_{ji}(\Delta\lambda) = \frac{E}{\Delta\lambda}n_j(E,z)\frac{A_{ji}}{4\pi^2}dz\,d\psi. \tag{17}$$

The photon emission rate Φ_{ji} resulting from charge exchange is obtained by integrating Eq. (17) over the rotation angle ψ and the depth z, taking into account the fact that the energy E of a particle with a rotation angle ψ generating an observed Doppler shift $\Delta\lambda$ is a function of both ψ and $\Delta\lambda$. Since n_j, the number density per energy range, depends explicitly on E, it is easier to express ψ as a function of E and to integrate Eq. (17) over the relevant $E_{min} \rightarrow E_{max}$ energy range defined below. This leads to the photon emission rate

$$\Phi_{ji}(\Delta\lambda) = 2\int_0^\infty\int_{E_{min}}^{E_{max}}\frac{E}{\Delta\lambda}n_j(E,z)\frac{A_{ji}}{4\pi^2}dz\,\frac{d\psi}{dE}\,dE \tag{18}$$

from which the line intensity $\Delta_{ji}(\Delta\lambda)$ can be derived using

$$\Delta_{ji}(\Delta\lambda) = \frac{hC}{\lambda_{ij}}\Phi_{ji}(\Delta\lambda). \tag{19}$$

The coefficient 2 in the right hand side of Eq. (18) comes from the symmetry around the direction $\psi = \pm\pi/2$ seen in Eq. (15).

Eq. (15) leads to

$$\sqrt{E} = \sqrt{\frac{m}{2}}\Delta\lambda\frac{c}{\lambda}\,/\,[\cos\theta\cos\alpha - \sin\theta\sin\alpha\sin\psi]. \tag{20}$$

Then, Eq. (20) leads to

$$d\psi = \frac{1}{2E}\sqrt{\frac{m}{2E}}\frac{c}{\lambda}\frac{\Delta\lambda}{\sin\theta\,\sin\alpha}\frac{1}{\cos\psi}dE, \tag{21}$$

and to

$$\cos\psi = \frac{\left[\sin^2\theta\sin^2\alpha - (\cos\alpha\cos\theta - \Delta\lambda\frac{c}{\lambda}\sqrt{\frac{m}{2E}})^2\right]^{1/2}}{\sin\theta\sin\alpha}. \tag{22}$$

The energy ranges are related to the rotation angle ranges by Eq. (21) and the expression for the photon emission rate depends on the beam geometry via the values of the parameters E_{min} and E_{max} in the following Eq. (23) that is derived from Eqs. (19), (21) and (22).

$$\Phi_{ji}(\Delta\lambda) = \frac{1}{4\pi^2}\frac{c}{\lambda}\int_0^\infty\int_{E_{min}}^{E_{max}}\sqrt{\frac{m}{2E}}A_{ji}\,n_j$$

$$\left[\sin^2\theta\sin^2\alpha - (\cos\alpha\cos\theta - \Delta\lambda\frac{c}{\lambda}\sqrt{\frac{m}{2E}})^2\right]^{-1/2}dz\,dE. \tag{23}$$

The parameters E_{min} and E_{max} are dependent on the geometry and are calculated in the next subsection. In all that follows the minimum energy E_{min} that contributes to the emission at a given $\Delta\lambda$ is computed for a beam distributed in energy at all depths from 0 to ∞. If the minimum energy E_m in the beam is greater than 0 (see Eq. (6)), then the minimum value to be used in Eq. (23) is not E_{min} as computed in the next two subsections but rather the greatest of the two E_m and E_{min} values.

2.3.1. Both blue and red shifted emissions are present

The emission is usually red shifted. However, blue shifted emission may also be present together with the red-shifted one. Blue shifted photons can be present for configurations such that $\tan\alpha\tan\theta \geq 1$, in such cases $\Delta\lambda < 0$, i.e. blue shifted emission is present for $\psi_1 < \psi < \pi/2$, where $\psi_1 = \arcsin(1/\tan\alpha\tan\theta)$. Since the Eq. (18) takes into account the symmetry around the direction $\psi = \pm\pi/2$. We then distiguish two subintervals, i.e. the subintervals $-\pi/2 \leftrightarrow \psi_1$ and $\psi_1 \leftrightarrow \pi/2$.

Interval $-\pi/2 \leftrightarrow \psi_1$*:*

The line intensity is given by Eqs. (19) and (23) with

$$E_{min} = \frac{m}{2}\Delta\lambda^2\frac{c^2}{\lambda^2}\frac{1}{(\cos\alpha\cos\theta + \sin\alpha\sin\theta)^2}\;(\psi = -\pi/2),$$

and

$$E_{max} = \infty\,(\psi = \psi_1).$$

Interval $\psi_1 \leftrightarrow \pi/2$*:*

At the limit ψ_1 of the interval $\psi_1 \leftrightarrow \pi/2$, $E_{max} = \infty$. The Eq. (14) shows that the highest possible amplitude of the blue

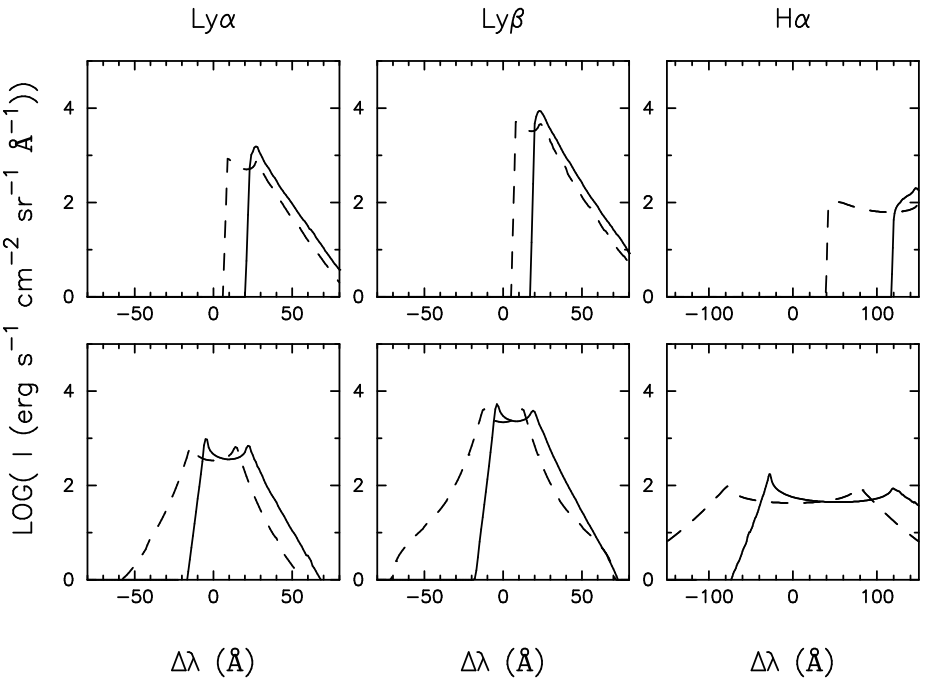

Fig. 2. θ-dependence of the non-thermal emission profiles of the Lyα, Lyβ and Hα lines in the case of bombardment by a power-law proton beam with a total input energy flux $\mathscr{F}_7 = 5 \times 10^{10}$ erg cm^{-2} s^{-1} above a low energy cutoff E_c = 300 KeV and of power index $\delta = 4$ for the quiet-Sun model C (Vernazza et al. 1981). Full lines are for θ= 10° (upper pannel) and 70° (lower pannel), while dashed lines are for θ= 45° (upper pannel) and 90° (lower pannel) respectively

shift generated by a proton of energy E and pitch angle α is obtained at the other limit $\psi = \pi/2$. In other words, the proton energy E_{min} needed to generate a photon with a blue shift $\Delta\lambda$ is minimum at $\psi = \pi/2$. Consequently the line intensity is given by Eqs. (19) and (23) with

$$E_{min} = \frac{m}{2}\Delta\lambda^2\frac{c^2}{\lambda^2}\frac{1}{(\cos\alpha\cos\theta - \sin\alpha\sin\theta)^2}\ (\psi = \pi/2),$$

and

$$E_{max} = \infty\ (\psi = \psi_1).$$

2.3.2. Only red or no shifted emission is present

If the beam configuration is such that $\tan\alpha\tan\theta < 1$, the line emission is always red shifted ($\Delta\lambda \geq 0$) and the line intensity is given by Eqs. (19) and (23) with

$$E_{min} = \frac{m}{2}\Delta\lambda^2\frac{c^2}{\lambda^2}\frac{1}{(\cos\alpha\cos\theta + \sin\alpha\sin\theta)^2},$$

and

$$E_{max} = \frac{m}{2}\Delta\lambda^2\frac{c^2}{\lambda^2}\frac{1}{(\cos\alpha\cos\theta - \sin\alpha\sin\theta)^2},$$

corresponding respectively to $\psi = -\pi/2$ and $\psi = \pi/2$.

3. Results

The purpose of our computation is mainly to show the wavelength dependence of the non-thermal emission of hydrogen in the Lyα, Lyβ and Hα lines caused through charge exchange by an oblique incident proton beam, with a pitch angle α around a vertical magnetic field, for different values of the heliocentric angle θ. We have also computed the atmospheric thermal emission for different atmospheric models. The same models as in FFH were used for comparison. These models are the semi-empirical flare models F1 and F2 given by Machado et al. (1980) and the quiet-Sun atmospheric model C given by Vernazza et al. (1981). The parameters we used for a power-law proton beam are a total energy flux $\mathscr{F}_1 = 5\times10^{10}$ erg cm^{-2} s^{-1} above a low energy cutoff E_c= 300 Kev and a power index $\delta = 4$. A version of our previous non-LTE code given in Fang et al.(1986) and Gan & Fang (1987) was used to compute all necessary self-consistent parameters (hydrogen density n_H and ionization x etc.). The background profiles of Lyα and Lyβ lines were also computed with this code.

Fig. 2 shows the θ-dependence of the non-thermal emissions of Lyα, Lyβ and Hα lines in the case of $\alpha = 30°$ for the model C. It can be seen that the line intensity peaks do not change much of position, while the line asymmetries vary obviously. As θ increases, the line peak shifts towards the line center. It should be mentioned that in the case of a vertical incident beam near the center of solar disk, the intensities of Lyα and Lyβ lines produced by charge exchange peak at a $\Delta\lambda$ of about 10 Å (see FHH), while in the case of an oblique incident beam, the position of the maximum intensities of these lines may be shifted differently, as indicated in Fig. 2. For instance, when $\alpha = 30°$ and $\theta = 10°$, the intensity of the Lyα and Lyβ lines peaks at $\Delta\lambda \simeq 20$Å, while the maximum intensity of the Hα line is at more than 100Å from line center. Compared with the results given by FFH, the maximum intensity decreases a little.

The results given by Fig. 2 are in agreement with the statement made in the previous section that for $\alpha + \theta < 90°$ all non-thermal line emission appears in the red wing and that for α +

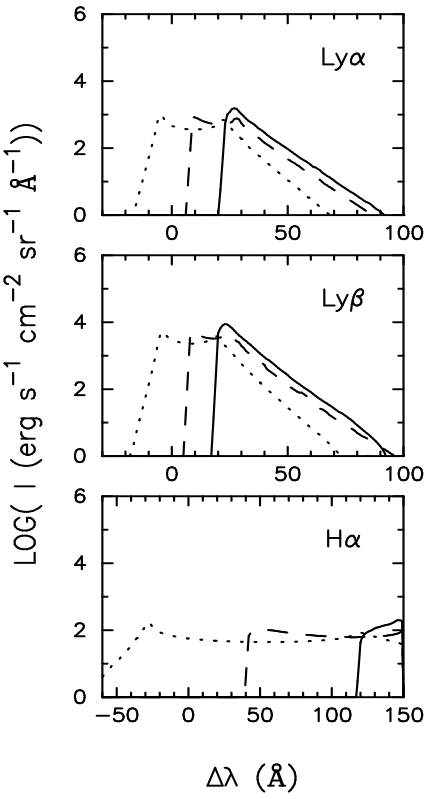

Fig. 3. α-dependence of the non-thermal emission profiles of the Lyα, Lyβ and Hα lines for θ= 30°. The proton beam parameters are the same as in Fig. 2, but α= 10° (full lines), 45° (dashed lines) and 70° (dotted lines)

$\theta > 90°$ a part of the emission appears in the blue wing, though the emission in the red wing remains dominant. When θ = 90°, the non-thermal emission is symmetrical around $\Delta\lambda$ = 0.

Fig. 3 shows the α–dependence of the non-thermal emission of the Lyα , Lyβ and Hα lines in the case of θ = 30°. It can be seen that, as the value of α increases, the emission peak shifts towards the line center and again when $\alpha + \theta > 90°$, blue shifted emission is present.

To compare the relative contributions of non-thermal and thermal emission, the Lyα and Lyβ line profiles are shown in Fig. 4 for the case α = 30° and θ = 70° and for the model C, which can be considered as a very initial state when a proton beam is bombarding the quiet-Sun atmosphere. It can be clearly seen that the non-thermal emission in both lines is much stronger than the thermal one, especially in the Lyβ line, where non-thermal emission is dominant and covers about 40 – 60 Å in width. That means that, due to non-thermal emission through charge exchange, just at the beginning of a major flare, in presence of a proton beam, there will be a "flash phase" in the Lyβ line. However, later in the flare, as shown in Fig. 5 for the model F1 which represents the atmosphere near the maximum state of a small flare or at the late phase of a major flare, the non-thermal emission of the Lyα line shall be less stronger than the thermal background, while the emission of the Lyβ line will still be

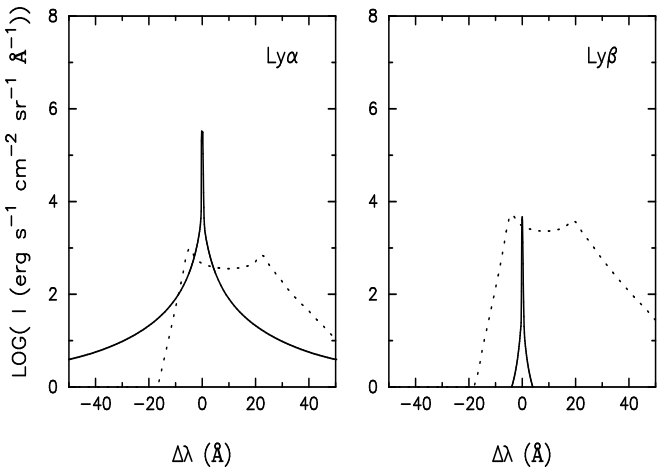

Fig. 4. Comparison of the thermal (full lines) and non-thermal (dotted lines, at α= 30°) emission profiles of the Lyα and Lyβ lines for the quiet-Sun model C (Vernazza et al. 1981) and for θ= 70°. The beam parameters are the same as in Fig. 2

strong. Thus, the Lyβ line is really a good diagnostic tool of proton beams with relative low energy.

Fig. 6 gives the non-thermal emission intensity for various atmospheric models, C, F1 and F2, at α = 30° and θ = 70°. It shows that the non-thermal emission is sensitive to the atmospheric structure. Similarly to the case of a vertical incident proton beam (see FHH), the non-thermal emission depends greatly on the coronal column mass m_0: the lower the m_0, the stronger the intensity of non-thermal emission is (from the model C through F1 to F2, m_0 increases). It should be mentioned that even in the case of the model C, the non-thermal Hα emission is three to four orders of magnitude weaker than the continuum background ($\sim 4.3 \times 10^6$ erg cm^{-2} s^{-1} sr^{-1} Å^{-1}), no matter the values of α and θ are. Thus, it would not be detectable with the present sensitivity of spectroscopic instruments.

4. Discussion and conclusion

We have computed the non-thermal Lyα, Lyβ and Hα line emission of superthermal hydrogen atoms produced by charge exchange in the case of the bombardment of the chromosphere by an oblique incident proton beam with a pitch angle α around a vertical magnetic field. Similarly to the vertical incident case (see FHH), it is shown again that the non-thermal Lyα and Lyβ line emissions are pronounced and detectable, while the non-thermal Hα emission is too weak to be observed. However, the results presented in this paper indicate that the line asymmetries depend greatly on the proton pitch angle α and on the heliocentric angle θ of the place bombarded by a proton beam. When $\alpha + \theta \geq 90°$, blue shifted emission is present, and for θ = 90° (at the solar limb), the non-thermal profiles even become symmetrical.

It should be mentioned that all the results presented above are valid for photons resulting from charge exchange not absorbed in the solar atmosphere. Only in a narrow wavelength

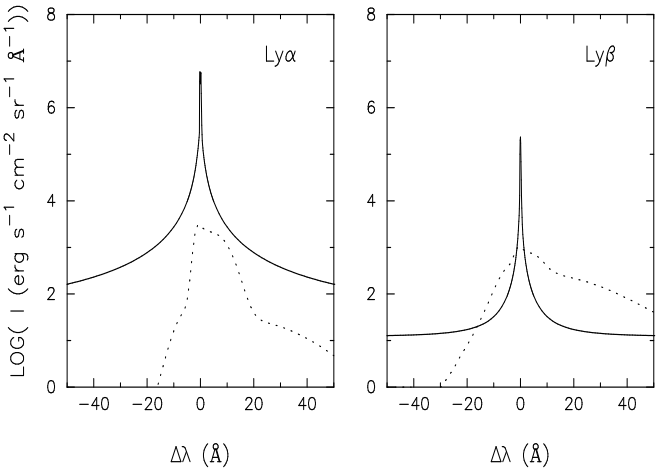

Fig. 5. Same as Fig. 4, but for the semi-empirical flare model F1 (Machado et al. 1980)

band centered on the unshifted line center with a half-width of about 2 Å is this hypothesis not valid. Outside this band, the absorption of the ambiant solar atmosphere can be neglected.

It must be emphasized that for all the lines considered non-thermal emission will be strong only at the very initial phase of the flare, when the coronal column mass is small. After the heating of the chromosphere, the coronal column mass increases rapidly, due to the ablation of chromospheric plasma, reducing strongly the proton energy in the layers emitting the hydrogen line spectrum.

Our results indicate that the intensity of the non-thermal emission induced by charge exchange depends on the parameters defining the proton beam ($\mathscr{F}_1$, E_c, δ and α), the atmospheric model and the heliocentric angle θ. Among these various parameters, only θ is known from observations. At the beginning of a flare, the quiet-Sun model can be used to represent the initial state of flare atmosphere. If the proton beam parameters can be determined by other methods, then spectral observations, especially the Lyβ line profiles, can be used to diagnose the proton pitch angle α. Indeed, our computations were only made for some given values of α. In fact, there is probably some distribution of α during solar flares. In this case, the line profile will be some kind of mixture of profiles corresponding to different α. In summary:

1. The asymmetry and the intensity of the non-thermal emission profiles generated through charge exchange by the bombardment of the solar atmosphere by an oblique incident proton beam strongly depend on the beam incident pitch angle α and on the angle between the direction of magnetic field and the line of sight. When $\alpha + \theta < 90°$, only red shifted emission appears, but as the value of $\alpha + \theta$ increases, the intensity peak will shift towards the line center. For $\alpha + \theta \geq 90°$, blue shifted emission will be present, and the lines will even become symmetrical when $\theta = 90°$.

2. Generally the intensities of non-thermal Lyα, Lyβ and Hα lines generated by an oblique incident proton beam are lower

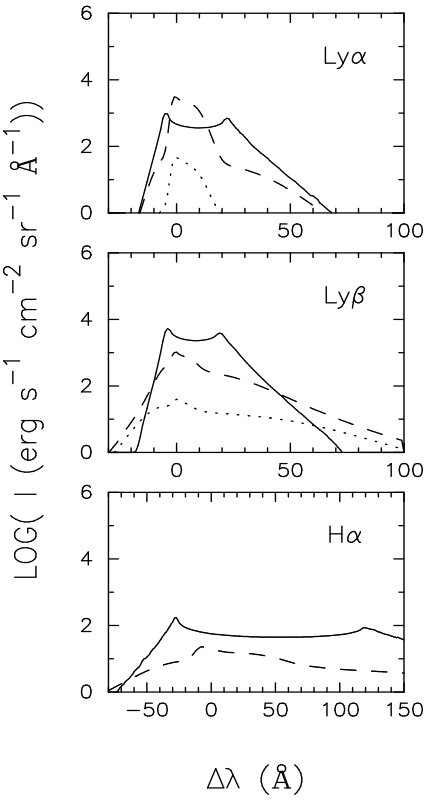

Fig. 6. Same as Fig. 3, but for the quiet-Sun model C (full lines), the flare model F1 (dashed lines) and F2 (dotted lines). In all case, α=30° and θ= 70°

than the one resulting from bombardment by a vertical beam. The non-thermal emission of Hα line is too small to be detectable. For the Lyα line, the non-thermal emission is also hard to observe, except just at the very initial phase of a flare. However, the line wing enhancement and broadening in the Lyβ line are significant, especially at the onset of a major flare. A "flash phase" can be expected. Thus, the Lyβ line is really a good diagnostic tool to detect non-thermal proton beam bombardment.

Acknowledgements. One author(C.F.) would like to express his sincere gratitude to the CNRS for supporting his stay and Paris Observatory for kind hospitality. We also thank the Referee for his valuable comments. This work was partly supported by a key project from the National Science Committee and the National Natural Science Foundation of P.R.China. Another author (J.C.H.) thanks also CNRS and NSFC for support and Nanjing university for kind hospitality.

References

Brekke P., Rottman G. J., Fontenla J., Juolge P. G., 1996, ApJ 468, 418
Brown J. C., 1971, Solar Phys. 18, 489
Brown J. C., Karlicky M., Mackinnon A. L., van den Oord G. H. J., 1990, ApJS 73, 343
Canfield R. C., and Chang C. R., 1985, ApJ 295, 275
Canfield R. C. et al. 1986, in Energetic Phenomena on the Sun. ed: M. R. Kundu & B. E. Woodgate, NASA cp-2439, p.3-i
Dennis B. R., 1988, Solar Phys. 118, 49

Dennis B. R., Uberall B. M., and Zarro D. M., 1993, Proc. IAU Colloq. 113 on Eruptive Solar Flares, Iguazu Falls, Argentina, Lecture Notes in Physics, 399, 714
Dennis B. R., and Zarro D. M., 1993, Solar Phys. 146, 177
Doschek G. A., Maritska J. T., Sakao T., 1996, ApJ 459, 823
Emslie A. G., Brown J. C., 1985, ApJ 295, 648
Emslie A. G., 1978, ApJ 224, 241
Emslie A. G., Hénoux J.-C., Mariska J. T., Newton E. K, 1996, ApJ 470, L131
Fang C., Huang Y. R., Hu J., Gan W. Q., 1986, in D. Neidig(ed.), The Lower Atmosphere of Solar Flares, NSO, Sunspot, NM., p.117
Fang C., Feautrier N., Hénoux J. -C, 1995, A&A 297, 854
Feldman U., Cheng C. C., Doschek G. A., 1982, ApJ 255, 320
Gan W. Q., Fang C., 1987, Solar Phys. 107, 311
Hénoux J. C., Chambe G., Smith D., Tamres D., Feautrier N., Rovira M., Sahal-Brechot S., 1990, ApJ 73, 303
Hénoux J. -C., Fang C., Gan W. Q., 1993, A&A 274, 293
Machado M. E., Arrett E. H., Vernazza J. E., Noyes, R. W., 1980, ApJ 242, 336
Neupert W. M. , 1968, ApJ 153, L59
Orral F. Q., Zirker J. B., 1976, ApJ 208, 618
Ramaty R., et al. 1980, in Solar Flares, ed. P. A. Sturrock, Boulder:University of Colorado Press, p. 117
Ramaty R., Mandzhavidze N., Kozlovsky B., Murphy R. J., 1995, ApJ 455, L193
Share G. H., Murphy R. J., 1995, ApJ 452, 933
Simnett G. M., Strong K. T., 1984, ApJ 284, 839
Syrovatskii S. I., Shmelova O. P., 1971, Soviet Astron. 16, 273
Vernazza J. E., Avrrett E. H., Looser R., 1981, ApJS 45, 635
Vogt E., Hénoux J.-C., 1996, Solar Phys. 164, 345
Zarro D. M., Mariska J. T., Dennis B. R., 1995, ApJ 440, 888

This article was processed by the author using Springer-Verlag LaTeX A&A style file *L-AA* version 3.